

Chapter 2

Molecular Beam Electric Field Deflection: Experimental Considerations

To understand the electric beam deflection method and the possibility to extract the dielectric properties of isolated clusters from these measurements, the essential components of the molecular beam apparatus are explained first. The experimental setup of a molecular beam apparatus build for beam deflection studies allows many variations and differs according to the kind of the studied cluster system. However, for the sake of simplicity we will introduce the basic experimental procedure with the help of an apparatus developed in our group. Possible modifications or instrumental variations will be indicated in the corresponding sub-chapters. First, the experimental procedure will be described to give the reader an idea how to experimentally realize these measurements and what components are required. Furthermore, we will phenomenologically introduce the measurement principle by discussing the observations made when performing a beam deflection experiment (Sect. 2.1). It will become clear, that the intensity distribution in the molecular beam differs between the field free measurements and those experimental runs when an electric field is applied. We will see that this difference can only be explained by a deflection of the clusters due to the electric field and that this deflection can qualitatively understood when taking the Stark effect of the cluster into account. A more detailed and quantitative discussion of this observation will be given in Chap. 3. In the subsequent sections the different components of the experiment are discussed in more detail. This includes the necessary vacuum setup (Sect. 2.2), the cluster generation in a cluster source (Sect. 2.3), the electric deflection unit (Sect. 2.4) and the mass spectrometer used to ionize and detect the neutral clusters (Sect. 2.5).

2.1 Experimental Setup and Measurement Principle

A schematic overview of the molecular beam apparatus which is used to study the dielectric properties of isolated clusters is shown in Fig. 2.1. First, the general experimental setup and the measuring principle is described. Important experimental details

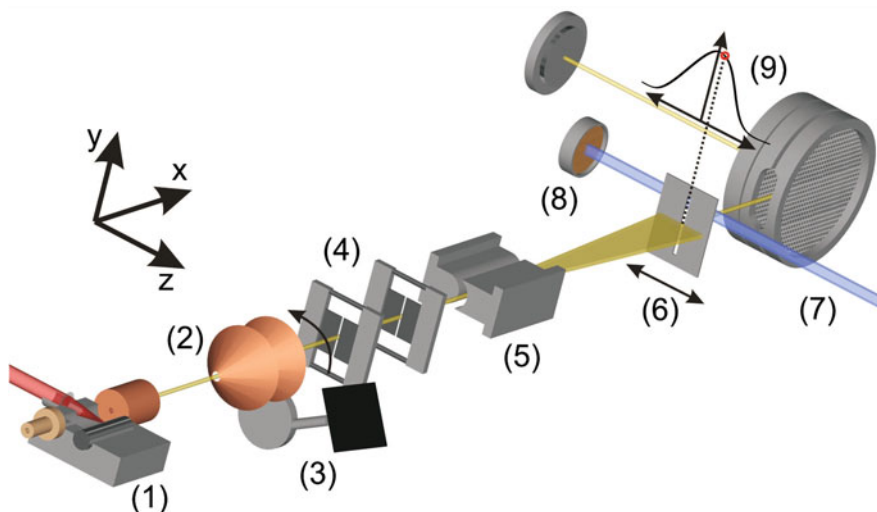


Fig. 2.1 Schematic setup of the molecular beam apparatus developed in our group: Cluster source with cooled expansion nozzle (1), double skimmer (2), shutter unit (3), collimators (4), electric deflection unit (5), movable slit aperture (6), F₂-Excimer laser (7), pyro-electric detector (8), time-of-flight mass spectrometer (9). The molecular beam is highlighted in yellow and the laboratory coordinate system is shown in the *upper left* part of the figure

are discussed in more detail in the following sections. Parts of the experimental setup have been described in references [1–3]. The experiment, which is repeated with a rate of 10 Hz, starts with the production of clusters in a laser vaporization source (1) (see also Sect. 2.3). Clusters are formed in a helium atmosphere after a laser pulse hits the target and are subsequently expanded through a nozzle into high vacuum. The cluster-helium mixture is thereby supersonically expanded and a molecular beam (Fig. 2.1, yellow) is formed [4], which is narrowed by two skimmers (2) with circular openings of 2 and 3 mm, respectively. In a molecular beam all particles exhibit a directed translation motion.¹ As a consequence of this directed motion and the absence of collision processes due to the low pressure (see also Sect. 2.2), the clusters can be considered as isolated particles [4]. The molecular beam passes a home-built shutter unit (3) [5]. At this point, it is possible to interrupt the particle beam at a well defined point in time, in order to measure the flight time of the clusters. The additional knowledge of the flight path (3.38 m) enables the determination of the particle speed v with an accuracy of (2–3)%. Next, the molecular beam passes a double collimator unit (4) resulting in a collimated 0.50-mm-wide (z -direction) and 3.00-mm-long (y -direction) rectangular beam shape. This rectangular beam enters the electric deflection unit (5) which will be described in Sect. 2.4. After leaving of the deflection unit (5) the clusters enter a 1.59-m-long area of free flight.

¹ This is in contrast to a thermal velocity distribution for which $\langle v_x \rangle = \langle v_y \rangle = \langle v_z \rangle = [4]$.

Subsequently, a, in z -direction, movable slit (6), which is 0.35 mm in width and 20.00 mm in height, is reached. The aperture exclusively allows a small portion of the molecular beam to proceed towards the ionization laser. These clusters are ionized by a F_2 -Excimer laser (7), whose fluence is monitored during a measurement by a pyro-electric detector mounted in the apparatus (8). The generated cluster ions are detected in a self-built time-of-flight mass spectrometer (9) and a photo-ionization mass spectrum is obtained (Sect. 2.5). Consequently, the described experiment allows the mass-resolved investigation of neutral clusters.

To be able to detect the influence of an inhomogeneous electric field on the clusters experimentally, it is necessary to record cluster intensities as a function of the movable slit position (6) and the electric field strength (5). First the position of the slit aperture is changed keeping the electric field constant. With the help of the before described collimators the molecular beam owns a predetermined intensity distribution along the z -axis, defined in the laboratory coordinate system.

The particle density is not constant along the z -axis, but will exhibit a maximum on the molecular beam axis² and will decrease when moving away from this position.³ This distribution of the particle density as a function of the z -position is called a molecular beam profile $\psi(z)$. Because the slit of the aperture is smaller than the dimensions of the molecular beam, only a small part of the beam is detected in the mass spectrometer. The actual number of clusters which can pass the slit depend on the aperture position. The particle density distribution of the molecular beam and, therefore, ψ can be measured sequentially by shifting the slit along the z -axis. Schematically, a beam profile without electric field (ψ_0 , dashed line) is shown in Fig. 2.2c. When applying a voltage to the deflection unit, the molecular beam profile is influenced by the electric field. This is schematically shown in Fig. 2.2c. In this example, the beam profile with field ψ_1 (black) is shifted and broadened

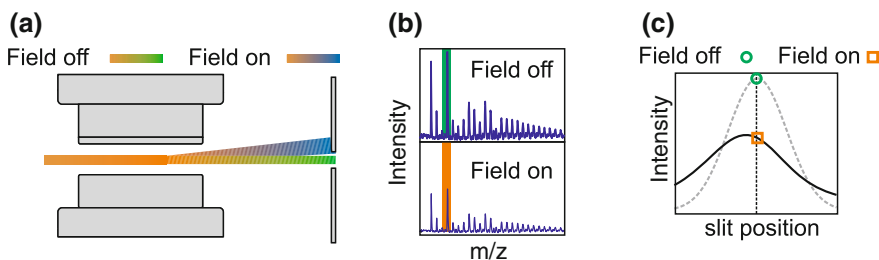


Fig. 2.2 **a** Schematic trajectory of the molecular beam with switched off and switched on electric field. **b** Mass spectra obtained for the two experiments shown in **a**. **c** Integrated signal intensity with the electric field switched off and on, respectively. The corresponding beam profiles ψ_0 (gray sketched) and ψ_1 are shown (black), too

² This position is chosen to be z_0 . Hence, it is convenient to use the relative z -scale $p = z - z_0$.

³ Furthermore, we note that for this experimental setup the particle density must be symmetric around z_0 . The observed intensity distribution can be described with a Gaussian function, what will be done in all what follows.

when compared to ψ_0 . In order to qualitatively understand this result, we want to discuss the experimental data acquisition and processing for a single cluster at a given slit position. If no electric field interacts with the clusters in the molecular beam, a photo-ionization mass spectrum is obtained as it is schematically shown in Fig. 2.2b for Si_N clusters (N is the number of atoms in the aggregate). In a next step, the mass spectrometric signal for an arbitrarily chosen cluster, e.g. Si_{11} (highlighted in green), is integrated and is plotted as a function of the slit position. As a consequence, the value of the molecular beam profile ψ_0 at this specific slit position is obtained (green circle in Fig. 2.2c). In the next step, the electric field is switched on and the intensity of the same cluster at the same slit position is measured again. A drop in intensity can be observed in Fig. 2.2b and a modified value for ψ_1 (orange square in Fig. 2.2c) is obtained.⁴ The only possible explanation that can rationalize this observation, is a deflection of the clusters in the molecular beam due to the applied electric field (see Fig. 2.2a). When deflected less clusters can pass the movable slit and the signal intensity will decrease. This effect can qualitatively be understood, if the dielectric response of the cluster in the electric field is taken into account. The applied electric field interacts with the electric moments of the neutral cluster (also called dielectric properties) and will influence the energy levels of the cluster, what is known to be the Stark effect [6]. Since the electric field is inhomogeneous (see Sect. 2.4) this interaction will lead to a net force acting on the cluster, resulting in the observed deflection. Therefore, the deflection is a measure of the Stark effect experienced by the cluster and is connected to the cluster's dielectric properties. By rationalizing the beam deflection we can, therefore, extract the dielectric properties from beam deflection experiments. A detailed theoretical description of the Stark effect and the beam deflection is given in Chap. 3.

2.2 Vacuum System

The experiments described in Sect. 2.1 require a high vacuum (HV) apparatus, ensuring the formation of a molecular beam of isolated clusters. At the pressure of below $\sim 10^{-6}$ mbar collisions between the clusters and the background gas can be avoided if the overall length traveled by the particles is small compared to the mean free path⁵ [4].

The experimental realization of the vacuum system is shown schematically in Fig. 2.3. In principle four chambers can be distinguished. The pressure realized during operation is described in the following. The laser vaporization source, in which helium pulses are introduced, is located in the source chamber (1). The working

⁴ To obtain the whole beam profiles the described experiment with and without field, needs to be repeated for several slit positions.

⁵ A rough estimate based on hard sphere collision cross section of N_2 shows that at 300 K and $\sim 10^{-5}$ mbar the mean free path is still about 10 m. Hence, for the described operating conditions collisions can be ruled out.

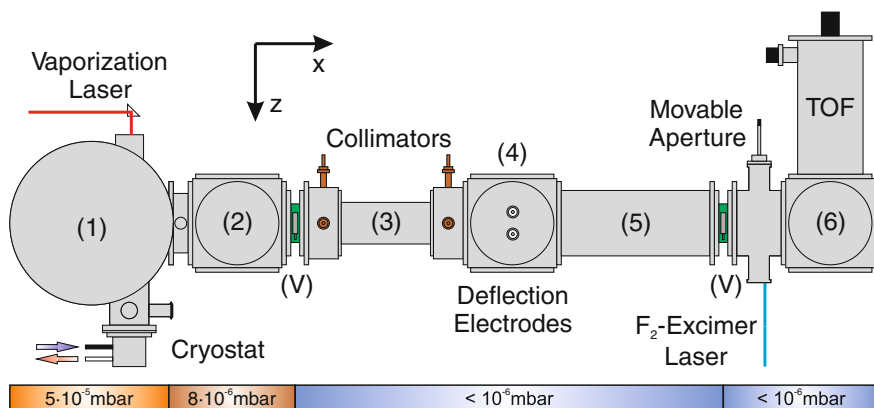


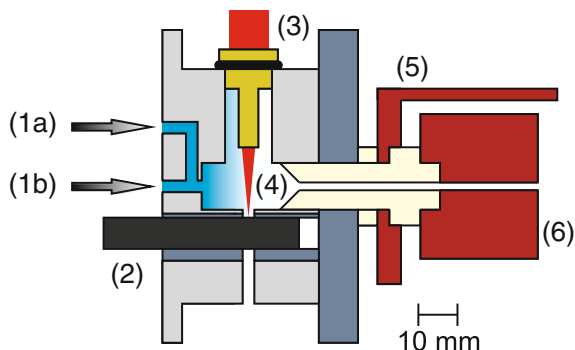
Fig. 2.3 Schematic view from the $+y$ direction on the molecular beam apparatus: Source vacuum chamber (1) with Nd:YAG laser beam (red, with prism) and He cryostat (blue and red arrow, cold and heated He stream), first differentially pumped chamber (2), flight tube (3) with collimators (bronze-colored), vacuum chamber for deflection electrodes (4), flight tube (5), vacuum chamber (6) with F₂-Excimer laser beam (cyan), slit aperture (gray-black) and time-of-flight (TOF) mass spectrometer. The high-vacuum (HV) valves (V) are shown in green. The pressure scale below the apparatus indicates the pressure during the experiment

pressure of $\sim 5 \cdot 10^{-5}$ mbar is reached by a diffusion pump (Leybold Heraeus, 12000 L/s) which itself is pre-pumped by a roots pump and an oil rotary vane pump. The source chamber (1) is connected by a double skimmer to the next differentially pumped chamber (2). The vacuum chamber (2) which among other things houses the shutter unit (see Sect. 2.1 and Fig. 2.1) is evacuated by a pumping stage consisting of a rotary vane and a diffusion pump (Leybold Heraeus, 1200 L/s) resulting in a pressure of $\sim 8 \cdot 10^{-6}$ mbar under operating conditions. The next vacuum chamber, in which the double collimator (3) and the deflection unit (4) as well as the first flight tube is located (5), can be separated from chamber (2) and (6) by means of two HV valves (V, green). The whole vacuum chambers (3), (4) and (5) are equipped with a rotary vane pump in combination with a diffusion pump (Edwards Diffstack 250/2000 m, 2000 L/s) achieving a base pressure below 10^{-6} mbar. The last vacuum chamber (6) contains the movable slit aperture, a MgF₂ window which allows the F₂-Excimer laser light to enter the vacuum chamber and the time-of-flight mass spectrometer. A pressure of less than 10^{-6} mbar is generated by a turbo molecular pump (Varian turbo-V 3K-T, 2050 L/s), pre-evacuated by a rotary vane pump.

2.3 Cluster Source Design

For the generation of clusters a whole series of sources have been developed. Beside sputter [7] and gas aggregation sources [8, 9], the laser vaporization technique is of special importance because clusters of very hard, non-conducting but also conducting

Fig. 2.4 Cross section of the laser vaporization source: Inert gas entries (1a and 1b, inert gas shown in blue), rotating and translating material rod (2), Nd:YAG-laser beam (red) focused by lens (3), cluster aggregation zone (4), radiation shield (5) and expansion nozzle (6)



materials can be generated. Therefore, most of the deflection experiments have been performed using laser vaporization sources and we will describe the source developed and used in our group in more detail.

The cluster source, which is shown in Fig. 2.4, is a home-built laser vaporization source based on the design of Smalley [10] and deHeer [11]. For the generation of clusters, helium, with a background pressure of ~ 8 bar, is injected through of a pulsed valve (typical opening times $350\text{--}1000\mu\text{s}$) in the source via the openings (1a) or (1b). The variable helium flow permits to modify the dwell time of the helium in the source. If gas enters through (1a) the formation of small clusters is preferred, while the use of (1b) is beneficial for the formation of larger aggregates. Typically $400\text{--}800\mu\text{s}$ after the helium pulse a Nd:YAG (yttrium aluminum garnet, pulse length 10 ns @ 1064 nm) laser with an energy between 40 and 100 mJ per pulse is focused by a lens (3) on a rotating and translating material rod (2). A few mono-layers of the material (2) are ablated by the intense laser pulse and a plasma is formed [12], which is rapidly cooled in the helium atmosphere, followed by the formation of clusters (4) by three-body collisions [7]. The pressure of some mbar helium in the source and the background pressure of $5 \cdot 10^{-5}$ mbar in the source chamber results in a supersonic expansion of the cluster-helium mixture through the nozzle with a 2 mm orifice and a total length of 61 mm (6). The first 36 mm of the nozzle is made of TeflonTM, while copper was used for the remaining 25 mm . In the copper block a heating element (max. 20 W) is integrated which is controlled by a PID regulator (proportional-integral-derivative, LakeShore 325). Plates made from oxygen-free high thermal conductivity cooper have been used to connect the copper block of the nozzle with a Helium closed cycle cryostat (Sumitomo Heavy Industries, 1 W @ 4.2 K). The temperature of the TeflonTM part of the nozzle remains close to room temperature,⁶ while the temperature of the copper block can be varied between 12 and 350 K . To minimize heat losses by radiation, a copper heat shield (5) surrounding the nozzle is precooled by the first cooling stage of the helium cryostat, which is held at $75\text{--}300\text{ K}$. As a consequence of the high pressure in the source, the cluster-helium mixture frequently collides with the nozzle wall [7] and, therefore,

⁶ Hence, the cluster source and the cooled part of the nozzle are thermally isolated.

thermalizes with the copper nozzle. After supersonic expansion, the temperatures of the different degrees of freedom of the clusters in the molecular beam are not longer in thermal equilibrium [4, 7]. Thereby, the rotational temperature (T_{rot}) can be lower than the nozzle temperatures, since the rotational degrees of freedom are cooled more effectively by cluster-wall and cluster-gas collisions (see [4, 7, 13, 14] for an in-depth discussion of supersonic expansions and the observed rotational, vibrational and translational temperatures and [15] for an example of typically observed rotational temperatures in supersonic jets). However, the vibrational temperature (T_{vib}) of the clusters in the molecular beam stays close to the nozzle temperature [16]. Consequently, by changing the nozzle temperature, the thermal excitation of the cluster skeleton can be influenced. For very low temperatures clusters can be considered as rigid, while at high nozzle temperatures clusters are thermally excited. These two limiting cases and the influence on the interpretation of the experimental results will be discussed in Chap. 3.

2.4 Deflection Unit

The determination of the electric susceptibilities of clusters requires an inhomogeneous electric field. In general static or dynamic fields can be used. First we will focus only on static deflection units. A more detailed description of the determination of dynamic dielectric properties with the help of time-dependent fields will be given in Sect. 5.1. For the generation of a static electric field, in principle, various electrode geometries can be used. Nevertheless, the by far most often used electrode geometry generates a so called “two-wire” field and we will focus our discussion on this electrode geometry [17, 18]. However, a couple of other electrode geometries have been used to perform deflection studies and some examples can be found in [19, 20].

The electrode geometry that generates an electric “two-wire” field and the corresponding coordinate system are shown in Fig. 2.5a. In analogy to the magnetic “two-wire” field [21] a convex electrode with radius a and a concave electrode with radius b are used. The z -component of the electric field strength is given by

$$E_z = \frac{K}{\sqrt{(a-y)^2 + z^2} \sqrt{(a+y)^2 + z^2}}, \quad (2.1)$$

and the corresponding field gradient

$$\frac{\partial E_z}{\partial z} = \frac{2 \cdot K \cdot z \cdot (a^2 + y^2 + z^2)}{[(a-y)^2 + z^2]^{3/2} [(a+y)^2 + z^2]^{3/2}} \quad (2.2)$$

can be obtained by deriving with respect to z . The parameter K present in Eqs. 2.1 and 2.2 is determined by the electrode radii $a = 3.8$ and $b = 4.0$ mm, as well as the potential difference U between the two electrodes [1]

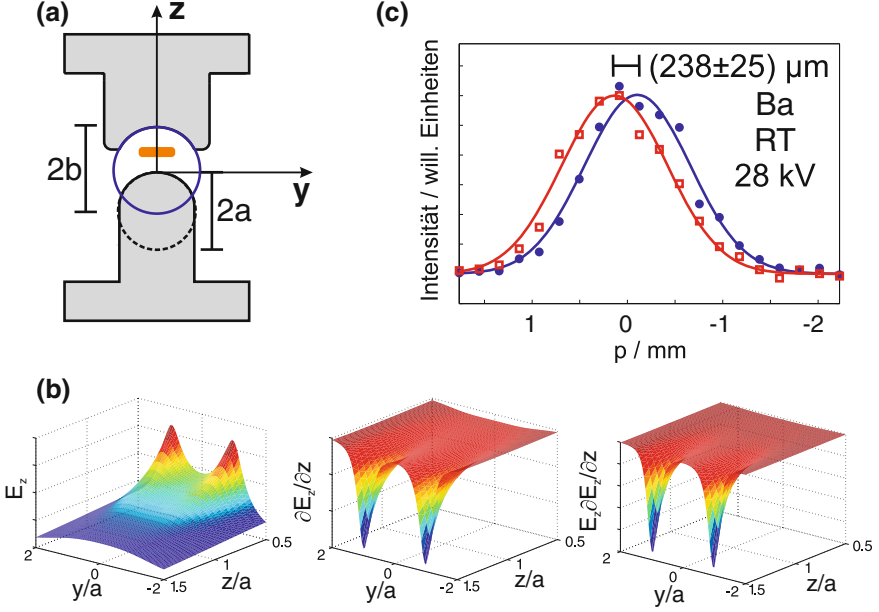


Fig. 2.5 **a** View from $+x$ direction on the deflection electrodes with a “two-wire” geometry. The molecular beam axis is highlighted in *orange*. The diameter of the concave and convex electrodes are given by $2a$ and $2b$, respectively. **b** Electric field strength (E_z), field gradient ($\partial E_z / \partial z$) and product of both quantities ($E_z \cdot \partial E_z / \partial z$) for the “two-wire” field geometry in arbitrary units as a function of y/a and z/a . **c** Typical experimental result for the beam deflection of barium atoms (speed ~ 1420 m/s, *blue dots* without field, *red squares* with field, Gaussian functions with the corresponding color are fitted to the data points) at room temperature (RT) and an applied deflection voltage of 28 kV. The position of aperture is abbreviated by p . A deflection of $(238 \pm 25) \mu\text{m}$ was observed

$$U = \frac{K}{a} \left[\arctan \left(\frac{a}{b} \right) - \frac{\pi}{4} \right]. \quad (2.3)$$

A special feature of the “two-wire” field is that the gradient $\partial E_z / \partial z$ as well as the product of the electric field E_z with the electric field gradient, which are responsible for the effects described in Sect. 2.1, remain nearly constant over the spatial dimensions of molecular beam (orange, Fig. 2.5a). In Fig. 2.5b E_z , $\partial E_z / \partial z$ and $E_z \cdot \partial E_z / \partial z$ are shown as a function of y/a and z/a . The position of the molecular beam relative to the electrodes is indicated in Fig. 2.5a in orange. Typically the molecular beam is located at $(1.1 - 1.2)a$ in z - and $(-0.35 - 0.35)a$ in y -direction for which $\partial E_z / \partial z$ as well as $E_z \cdot \partial E_z / \partial z$ change only about $\sim 5\%$. Therefore, the force experienced by the particles is to a good approximation independent of their position in the molecular beam (see Eq. 3.3). In order to quantify the observed beam deflection it is necessary to introduce an apparatus constant (Eq. 2.4). It turns out to be useful to introduce the constant

$$\gamma = \frac{\sigma}{U^2} E_z = \frac{l_1^2 + l_1 l_2}{U^2} \frac{\partial E_z}{\partial z} E_z, \quad (2.4)$$

which is independent of the applied deflection voltage. The quantities l_1 and l_2 in Eq. 2.4 are the electrode length (150 mm) and the distance of free flight (1590 mm, see Sect. 2.1), respectively. Furthermore, the constant σ is introduced which depends on U but often it is more convenient to use σ when discussing the beam deflection or the force experienced by particles (see Eqs. 3.3 and 3.5). The calibration constant can be determined by measuring the beam deflection of a particle with well characterized dielectric properties. For our experimental setup we used the barium atom [22, 23]. A typical beam profile obtained for Ba is shown in Fig. 2.5c. The average of five measurements gave a value of $\gamma = (2.8 \pm 0.2) \cdot 10^7 \text{ m}^{-1}$ in very good agreement with theoretical predictions taking Eqs. 2.1 and 2.2 into account [1].

2.5 Position-Sensitive Mass Spectrometry

For the size selected detection of clusters a mass spectrometer (MS) is required. In principle all types of mass spectrometers can be used to perform beam deflection measurements. Nevertheless, in practice mostly time-of-flight (TOF) mass spectrometers are used but also several studies with quadrupole MS [8, 19] are known. The advantage of a TOF-MS is that all cluster species in a molecular beam can be probed at the same time. If the molecular beam profiles are recorded serially by scanning the molecular beam with the help of an aperture, a TOF-MS with space focusing is used [24]. In our setup the neutral clusters pass the aperture and are subsequently ionized by a F_2 -excimer laser (wavelength 157 nm, see Fig. 2.1). The laser intensity profile shows a rectangular cross section from $20 \times 10 \text{ mm}^2$ with an average energy per pulse of $150 \mu\text{J}$. The pulse energy can be measured during the experiment by a pyro-electric detector (see Fig. 2.1). The ionized clusters enter the acceleration region of the TOF-MS, in which the clusters are deflected orthogonal to their original flight direction by applying voltages of 3–4 kV in about hundred nanoseconds by high voltage switches. After a 35 cm-long region of free flight the clusters are post-accelerated on an Even cup [25]. The secondary electrons generated are converted in photons by a fluorescence plate. The photons are detected and multiplied by photomultiplier stage. Typically a mass resolution of better than 100 is reached. If a TOF-MS with a reflectron is used the mass resolution could be further enhanced [26].

For the determination of the molecular beam profiles ψ_0 and ψ_1 , about 60 experiments are performed at 20 randomly selected slit positions. This means at each slit position on average three experiments are performed. One experiment consists of measuring the photo-ionization mass spectrum with and without electric deflection field at a given slit position, while each mass spectrum is the average of 100–200 pulses.

As an alternative to serially scanning the molecular beam, position sensitive TOF-MS techniques have been used [27–29]. In this approach, the molecular beam is not scanned with the help of aperture, but the molecular beam profile is reconstructed from the flight time. For that purpose the space focusing conditions must be slightly altered, so that different starting positions manifest in different flight times,

i.e. a molecular beam deflection and broadening manifests in a deflection and broadening of the time-of-flight signal, respectively. The big advantage of this method is that molecular beam profiles are measured at the same time for all positions without scanning a slit aperture, thereby increasing the signal-to-noise ratio and decreasing the duration of the experiment. However, the serial scanning mode is, in comparison to the position sensitive TOF-MS, more sensitive to small deflections, allowing the investigation of clusters with a small Stark effect or with very high mass. Whether position sensitive detectors will unify the advantages of both operation modes, remains open to future investigations [30].

References

1. Schäfer S (2008) Der Stark-Effekt als Werkzeug zur Strukturaufklärung isolierter cluster. Dissertation, Fachbereich Chemie, TU Darmstadt.
2. Mehring M (2007) Elektrische Molekularstrahlexperimente am Beispiel kleiner neutraler Bariumspezies. Diplomarbeit, Fachbereich Chemie, TU Darmstadt
3. Rohrmann U (2008) Magnetisches Verhalten reiner und Mangan-dotierter Zinn-Cluster. Master's thesis, Fachbereich Chemie, TU Darmstadt
4. Scoles G (1988) Atomic and molecular beam methods, vol 1. Oxford University Press, New York
5. Scholten RE (2007) Rev Sci Instrum 78:026101
6. Scheffers H, Stark J (1934) Phys Z 35:625
7. Haberland H (1995) Clusters of atoms and molecules I. Springer, Berlin
8. Moro R, Rabinovitch R, Xia C, Kresin VV (2006) Phys Rev Lett 97:123401
9. Carrera A, Mobbili M, Marceca E (2009) J Phys Chem A 113:2711
10. Dietz TG, Duncan MA, Powers DE, Smalley RE (1981) J Chem Phys 74:6511
11. Milani P, de Heer WA (1990) Rev Sci Instrum 61:1835
12. Bergmann L, Schaefer C (1992) Experimentalphysik 5: Vielteilchen-Systeme. Walter de Gruyter Verlag, NewYork
13. Mate B, Tejeda G, Montero S (1998) J Chem Phys 108:2676
14. Montero S (2013) Phys Fluids 25:056102
15. Lenzer T, Bürsing R, Dittmer A, Panja SS, Wild DA, Oum K (2010) J Phys Chem A 114:6377
16. Pokrant S (2000) Phys Rev A 62:051201
17. Ramsey NF (1956) Molecular beams. Oxford University Press, Oxford
18. Pauly H (2000) Atom, molecular and cluster beams II. Springer, Berlin
19. Sievert R, Cadez I, Van Doren J, Castleman AW (1984) J Phys Chem 88:4502
20. Imura K, Ohoyama H, Kasai T (2004) Chem Phys 301:183
21. Rabi II, Millman S, Kusch P, Zacharias JR (1939) Phys Rev 55:526
22. Schäfer S, Mehring M, Schäfer R, Schwerdtfeger P (2007) Phys Rev A 76:052515
23. Schwartz HL, Miller TM, Bederson B (1974) Phys Rev A 10:1924
24. Wiley WC, McLaren IH (1955) Rev Sci Instrum 26:1150
25. Bahat D, Cheshnovsky O, Even U, Lavie N, Magen Y (1987) J Phys Chem 91:2460
26. Mamyrin B (2001) Int J Mass Spectrom 206:251
27. de Heer WA, Milani P (1991) Rev Sci Instrum 62:670
28. Knickelbein MB (2001) J Chem Phys 115:5957
29. Antoine R, Rayane D, Allouche AR, Aubert-Frecon M, Benichou E, Dalby FW, Dugourd P, Broyer M, Guet C (1999) J Chem Phys 110:5568
30. Rahim MAE, Antoine R, Arnaud L, Barbaire M, Broyer M, Clavier C, Compagnon I, Dugourd P, Maurelli J, Rayane D (2004) Rev Sci Instrum 75:5221

Dielectric Properties of Isolated Clusters

Beam Deflection Studies

Heiles, S.; Schäfer, R.

2014, VI, 100 p. 34 illus., 27 illus. in color., Softcover

ISBN: 978-94-007-7865-8